Hindawi
Adsorption Science & Technology
Volume 2023, Article ID 5594717, 11 pages
https://doi.org/10.1155/2023/5594717

Research Article

Removal of Nitrate Nitrogen in Groundwater by Attapulgite Loaded with Nano-Zero-Valent Iron

Yangyang Zhang,[1,2,3] **Yunfeng Tan**,[1] **Bo Zu**,[1] **Xiaotian Zhang**,[1] **Chunli Zheng**,[4] **Zishen Lin**,[4] **Fei He**,[4] **and Kejun Chen**[5]

[1]*College of River and Ocean Engineering, Chongqing Jiaotong University, Chongqing 400074, China*
[2]*Chongqing Bureau of Geology and Mineral Resources, Chongqing 401121, China*
[3]*Chongqing Gangli Environmental Protection Co., LTD., Chongqing 400042, China*
[4]*Department of Environmental Science and Engineering, Xi'an Jiaotong University, Xi'an 710049, China*
[5]*China Merchants Ecological Environmental Protection Technology Co., LTD., Chongqing 400067, China*

Correspondence should be addressed to Bo Zu; culangg@gmail.com

Received 23 November 2022; Revised 14 January 2023; Accepted 27 January 2023; Published 15 February 2023

Academic Editor: Szabolcs Pap

Nano-zero-valent iron (nZVI) can be used to remove nitrate nitrogen (NO_3-N) from groundwater. However, it has low reduction efficiency owing to its oxidation and aggregation characteristics. Thus, nZVI-loaded material is used to alleviate these drawbacks. In this study, nZVI-coated attapulgite (ATP) was prepared for the removal of NO_3-N from groundwater. ATP-nZVI was prepared using the chemical liquid deposition-coreduction method. The prepared materials were characterized by SEM, XRD, and XPS analyses, which confirmed that the aluminum silicate particles in the ATP structure are effective carriers of nZVI and effectively inhibit self-consumption caused by the oxidation and aggregation of nZVI. The batch experiments examined experimental samples containing 30 mg/L nitrate and analyzed the effects of various parameters, including the material, mass ratio, initial pH, initial temperature, and coexisting anions on the NO_3-N removal efficiency. The results showed that the optimal removal rate of the composite was 78.61%, which is higher than that using the same amount of ATP, iron powder, and nZVI. When the mass ratio of ATP to nZVI was 1 : 1, the NO_3-N removal efficiency was the highest. When the pH value increased from 3 to 9, the NO_3-N removal rate decreased, while an increase in the reaction temperature promoted NO_3-N removal. The order of the inhibitory effect of coexisting anions on NO_3-N removal by various nanoions was $PO_4^{3-}>CO_3^{2-}>SO_4^{2-}>Cl^-$. The adsorption kinetic model fitting results indicated that the chemisorption of electron exchange between ATP and nZVI in NO_3-N removal was the main rate-limiting step in the reaction. This study demonstrates the potential of the prepared ATP-nZVI composite for NO_3-N removal from groundwater.

1. Introduction

Industrial discharges, urban activities, pesticides and fertilizer usage in agriculture, and disposal of waste have led to groundwater pollution becoming a serious problem, wherein nitrate is an important cause of groundwater pollution ([1, 2]. Long-term exposure to high nitrate levels poses varying degrees of risk to human health, such as the conversion of hemoglobin to methemoglobin, which depletes oxygen levels in infant blood, suppresses thyroid function, and forms nitrosamines that can cause cancer [3]. In 2017, the World Health Organization's International Agency for Research on Cancer listed nitrate and nitrite as 2A carcinogens [4]. China's new standard implemented in 2006 revised the maximum allowable limit for nitrate in drinking water to 10 mg/L (identical to that in the USA) [5]. Therefore, developing composite materials capable of adsorbing and oxidizing nitrate is important when remediating nitrate contamination in groundwater.

Nanomaterials have large surface areas and a small particle size [6] and can be injected into polluted groundwater for in situ repair. Synthesizing nanomaterials for removing

nitrate from groundwater has become a focal topic of research studies [7]. Nano-zero-valent iron (nZVI) has been widely adopted as a good electron-donating material and preliminarily tested for removing nitrate from groundwater owing to its high removal efficiency [8], generation of fewer intermediate products in the process, and environmental friendliness [9–11]. However, the disadvantages of nZVI, such as easy oxidation by nontarget chemicals and particle aggregation, limit its direct application in the remediation of nitrates in polluted groundwater. These disadvantages usually lead to a rapid decrease in catalytic activity and material waste and, thus, limit its cost-effectiveness [12]. To overcome these challenges, several studies have attempted to improve the stability and dispersibility of nZVI particles (Table 1), and many modifications have been reported for nZVI or composites between nZVI and other adsorbents. Vicente-Martinez et al. [13] successfully prepared silver-functionalized magnetic nanoparticles and revealed their ability to remove nitrates from water in a relatively short duration, with an adsorption efficiency of 100%. Liu et al. [14] used Fe0/Pd/Cu nanocomposites to remove groundwater nitrate and found that the introduction of Pd and Cu improved NO_3-N removal rate and also reduced the amount of ammonia nitrogen produced. Ghosh et al. [15] enhanced the aerobic stability of nanoparticles by synthesizing them in a medium consisting of a viscous solvent, glycerol, and water. Furthermore, they showed that the pollutant removal rate was higher under acidic conditions than under alkaline conditions.

As a natural mineral, attapulgite (ATP) is a typical crystalline hydrated magnesium silicate [16], which can promote NO_3-N removal by nZVI in aqueous solution. Compared with other clay minerals, not only is ATP abundant in reserves and inexpensive but it also has more efficient adsorption characteristics [17], porous structure, large specific surface area, and reasonable cation exchange capacity [18]. These properties can be used for the adsorption of ferrous or ferric oxide and further reduction of nZVI [19]. Several studies have assessed the performance and pollutant removal capacity of ATP-loaded nZVI composites [20–23] and showed that ATP-loaded nZVI composites have improved interfacial effect between materials and enhanced ability to remove pollutants.

In this study, ATP was used as a porous material carrier to synthesize ATP-nZVI using a liquid-phase reduction method. The effect of the interaction between ATP and nZVI on NO_3-N removal from simulated groundwater was evaluated. The overall objectives of this study were to (1) characterize ATP-nZVI composites; (2) determine the influence of nZVI on the ATP mass ratio, initial pH, initial temperature, and coexisting anions for NO_3-N removal; and (3) further understand the underlying NO_3-N removal mechanism of ATP-nZVI. Our results provide a theoretical basis and technical support for the remediation of NO_3-N polluted groundwater.

2. Materials and Methods

2.1. Experimental Materials. The chemicals used in this study, i.e., sodium nitrate ($NaNO_3$), hydrochloric acid (HCl), sodium borohydride ($NaBH_4$), sodium hydroxide (NaOH), and anhydrous ethanol (CH_3CH_2OH), were provided by Sinopharm Chemical Reagent Co., Ltd. (China). Phenylcarbazide ($C_{13}H_{14}N_4O$) and potassium iodide (KI) were purchased from Tianjin Fuchen Chemical Reagent Factory (China). Sodium nitrite ($NaNO_2$), sodium carbonate (Na_2CO_3), sulfamic acid (NH_2SO_3H), and ferric chloride hexahydrate ($FeCl_3{\cdot}6H_2O$) were obtained from Tianjin Damao Chemical Reagent Factory (China). All chemicals were of analytical grade. All solutions were prepared in deionized water. N_2 (99.9% purity), purchased from Xi'an Oxygen Source Oxygen Cylinder Sales Company (China), was blown into all prepared solutions for deoxygenation.

2.2. Preparation of ATP-nZVI Composites. In attapulgite purification, the raw ATP was ground and filtered through a 200-mesh sieve and then incubated in an oven set at 105°C for 240 min to remove excess water [23–26]. The removal of water from attapulgite required 10 g attapulgite being placed into 200 mL deionized water. We then added 3.2 g sodium hexametaphosphate as a dispersant [23, 26]. The mixture was then subjected to ultrasonic magnetic stirring for 15 min, so that the attapulgite powder, under the action of the dispersant, quickly dispersed to prevent agglomeration. Next, the mixture was centrifuged at 3,000 rpm for 15 min to obtain the upper milky white phase. Finally, the precipitate was dried at 105°C for 240 min and ATP was filtered through a 200-mesh sieve to achieve pure ATP.

We used the liquid-phase chemical reduction method [27], where deionized water (250 mL) was weighed into a three-necked flask using a graduated cylinder. Then, nitrogen was introduced to the deionized water for 30 min to remove dissolved oxygen (DO). Then, 4.8214 g $FeCl_3{\cdot}6H_2O$ was weighed and added to the three-necked flask containing 250 mL of deionized water. Subsequently, 1 g ATP was added and stirred vigorously (500 rpm) for 30 min. Then, 3 g $NaBH_4$ was dissolved in 100 mL deionized water and the $NaBH_4$ reagent was dropped into a three-necked flask with a peristaltic pump at a speed of 1 drop/s. The mixture was stirred for 40 min to ensure that the $NaBH_4$ and Fe^{3+} had fully reacted, as shown in Equation (1), and the entire process was carried out under a nitrogen atmosphere:

$$4Fe^{3+} + 3BH_4^- + 9H_2O \longrightarrow 4Fe^0 + 3H_2BO_3^- + 12H^+ + 6H_2. \quad (1)$$

After the reaction, the precipitate was washed with absolute ethanol (when nZVI is dispersed in the attapulgite matrix, latter's hydroxyl group provide a passivation contact to impart spatial stability, thereby preventing nZVI aggregation) [28] two to three times to obtain a black suspension. Finally, suction filtration was performed using a vacuum pump and ATP-nZVI composite was obtained as solid particles.

2.3. ATP-nZVI Characterization. The surface morphologies and structures of ATP, nZVI, and ATP-nZVI were observed using scanning electron microscopy (SEM) (Zeiss, Zeiss Sigma500, Germany). To further understand the material surface composition, an X-ray diffractometer (XRD) (Bruker, BRUKER D8 ADVANCE, Germany) was

Table 1: Comparison of NO_3-N removal by various loaded nano-zero-valent iron materials.

Load materials	C_0 (mg/L^{-1})	Initial pH	T (K)	Removal rate (%)	Cost	References
nZVI without support	100	3	313	40	Low	[48]
Pd/Cu	30	7	313	63.2	High	[49]
Composites of boiling stone	30	7	298	43	High	[50]
Acticarbon	60	3	298	89.7	Middle	[51]
Zeolite	100	5.5	298	84.3	Middle	[52]
Attapulgite	30	5	298	78.6	Low	This study

used to analyze the material and determine the crystal structure while verifying the successful loading of ATP onto nZVI. The ATP-nZVI and ATP-nZVI composites obtained after the reaction with nitrate were identified by X-ray photoelectron spectroscopy (XPS) (ESCALAB Xi+, Thermo Scientific, USA).

2.4. Batch Experiments. All batch experiments were conducted in 50 mL conical flasks. To simulate the real environment and the dark and anaerobic environment of groundwater, nitrogen gas (DO < 0.5 mg/L) was injected into the solution before the reaction. The reaction flask was wrapped with aluminum foil and evaluated under dark conditions. Studies have suggested that the nitrate pollution range of groundwater in the Chongqing area is approximately 30 mg/L; therefore, 30 mg/L $NaNO_3$ was added to simulated nitrate wastewater.

A series of experiments were conducted to study different materials (ATP, Fe, nZVI, and ATP-NZVI), the mass ratio of nZVI to ATP (1 : 0.5, 1 : 1, 1 : 3, and 1 : 5), initial pH of the solution (3, 5, 7, and 9), solution temperature (15, 25, and 35°C), and coexisting anions (anion concentration and nitrate nitrogen ion ratio were all 4 : 1). Briefly, 50 mL $NaNO_3$ containing DI water was placed in a conical flask and 75 mg preparation material was added to it. The mixture was placed in a thermostatic shaking water bath (160 rpm) at 25°C to perform the removal experiment. Sample aliquots were obtained using a 10 mm syringe at regular intervals. The reaction was performed for 150 min, and samples were collected every 10 min for the first 60 min. Following this, samples were obtained every 30 min for the last 90 min of the experiment (a total of eight aliquots of 0.5 mL each). The samples were filtered through a 0.45 μm syringe filter, and the filtered liquid was placed in the sampling bottle.

In this study, the temperature comparison experiment was conducted at 35°C, while the remaining experiments were conducted at 25°C. The temperature of groundwater varies with the region. Studies have reported that global warming had affected the groundwater layer to a certain extent. Tissen et al. [29] showed that the temperature of groundwater in central Europe generally ranges between 2 and 46°C. Ciardelli et al. [30] also performed a series of experiments to explore groundwater, and except for evaluating the effect of different temperatures, their experiments were performed at 25°C. Therefore, we selected 25°C as the representative groundwater temperature.

2.5. Analytical Methods. The NO_3-N, NH_4-N, and NO_2-N concentrations in the solution were measured using a UV spectrophotometer (PerkinElmer, PELambda950, USA) ([23, 31]. The concentration of NO_3-N was measured at 220 nm; the value of NO_3-N was corrected at 275 nm, with a detection limit of 0.08 mg/L. The concentration of NH_4-N was analyzed at 425 and 540 nm, with detection limits of 0.025 and 0.025 mg/L, respectively. The NO_2-N concentration was detected at the lower limit, with a detection limit of 0.003 mg/L.

2.6. Statistical Methods. All experiments were performed in triplicate. The data are expressed as the mean ± standard deviation. As shown in Equation (2). XPS phases were analyzed using the Avantage software (version 5.948, Thermo Fisher Scientific). The adsorption kinetics data were fitted using the Origin software (Origin Lab, 2018, USA). The adsorption kinetic model is described in the Supporting Information (SI, Section 1).

$$R(\%) = \left(1 - \frac{C_t}{C_0}\right) \times 100, \tag{2}$$

where C_0 is the initial nitrate concentration and C_t is the nitrate concentration at time t.

3. Results and Discussion

3.1. Characterization of ATP-nZVI and Interaction between ATP and nZVI. Figure 1 shows the SEM images of ATP, nZVI, ATP-nZVI, and nitrate-laden ATP-nZVI. The ATP was characterized by rod- and block-like structures (Figure 1(a)) while nZVI was characterized by spherical particles of varying sizes. Owing to the small diameter of the nanoiron particles, there was an interaction force between the particles, which led to the aggregation of the nZVI particles (Figure 1(b)). Following ATP loading, the ATP-nZVI particles exhibited better dispersion than the nZVI particles. The small nZVI particles were distributed on the surface and pores of ATP. This resulted in a higher surface area and a greater number of reaction sites (Figure 1(c)). The particle size of nitrate-laden ATP-nZVI increased after the reaction, and notable agglomeration was observed. During ATP adsorption, NO_3-N is adsorbed to the surface and the oxidation reaction occurs on nZVI, resulting in the formation of iron oxide and iron hydroxide on nZVI surface. These results demonstrate the successful preparation of ATP-

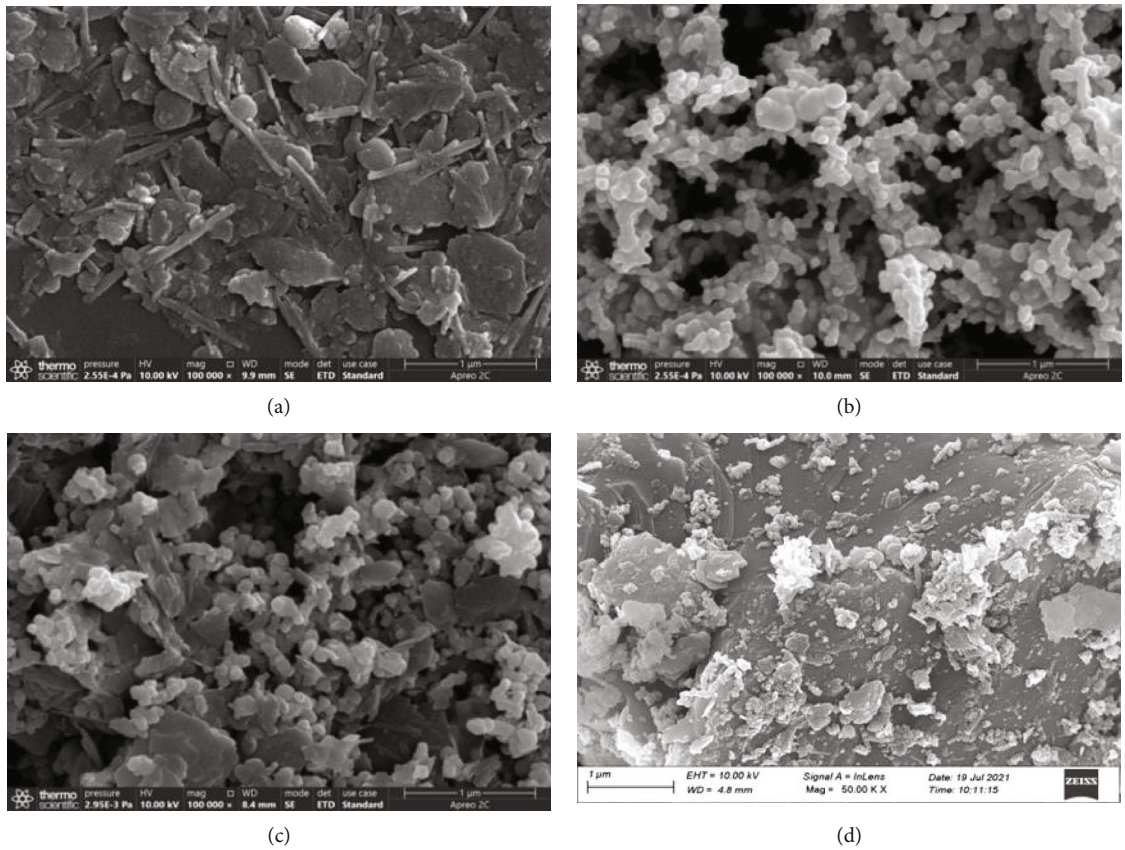

Figure 1: SEM images of (a) ATP, (b) nZVI, (c) ATP-nZVI, and (d) nitrate-laden ATP-nZVI. ATP: attapulgite; ATP-nZVI: nano-zero-valent iron-coated attapulgite; nZVI: nano-zero-valent iron.

nZVI composites and that NO_3-N was effectively adsorbed on ATP-nZVI surface.

Figure 2 shows the XRD patterns of ATP, nZVI, ATP-nZVI, and nitrate-laden ATP-nZVI, with characteristic diffraction peaks for ATP at $2\theta = 19.82\circ$, 21.68°, and 26.69° (Figure 2(a)). ATP is a natural mineral composed of SiO_2 [23]. In Figure 2(d), a 2θ of 44.8° was observed in the nZVI spectrum, confirming the existence of α-Fe^0, the characteristic diffraction peak of nZVI ([32–34]. When ATP was loaded with nZVI, typical diffraction peaks for ATP and nZVI appeared in the XRD spectrum of ATP-nZVI. The loaded material increased the crystallinity of α-Fe^0 because iron can be adsorbed on aluminum silicate sites. The doping of SiO_2 increases the crystallinity of nZVI [20, 22, 35]. We confirmed that the aluminum silicate particles in the ATP structure functioned as effective carriers of nZVI, which confirmed the successful preparation of the ATP-nZVI composites.

Figure 3 shows the XPS results before and after NO_3-N removal using ATP-nZVI. The binding energies of Fe 2p at 725.4 and 712.9 eV were assigned to Fe_2O_3 and Fe_3O_4, respectively. However, a signal peak of Fe^0 was noted at a binding energy at 707.1 eV in Figure 3(a), but not in Figure 3(b). This was attributed to the participation of Fe^0 in nZVI in the reduction reaction to remove nitrate nitrogen [36].

3.2. Comparison of NO_3-N Removal Rates by Different Materials. The NO_3-N removal efficiencies of ATP, Fe (particle sizes: 0.075-0.09 mm), nZVI, and ATP-nZVI were investigated. In the solution containing an initial NO_3-N concentration of 30 mg/L, the NO_3-N removal rates were 10.75%, 41.37%, 55.48%, and 78.61%, respectively, (Figure 4), after 150 min. The ATP and iron powder also exhibited an NO_3-N removal effect; however, it was not satisfactory since electrostatic repulsion occurred between ATP and NO_3-N [20, 22], whereas iron powder was easily oxidized and had a small surface area. However, ATP-nZVI and nZVI had 5.2- and 7.3-fold higher NO_3-N removal rates, respectively, than that of ATP. This indicated that the fine particles of nZVI enabled the exposure of its active sites, thereby promoting NO_3-N removal, whereas ATP-nZVI composites inhibited the agglomeration of nZVI particles via ATP loading and removed nitrates by reduction, adsorption, and surface complexation. These results confirmed that nZVI played a significant role in the removal of reductive NO_3-N.

3.3. Influence of nZVI on ATP Mass Ratio. To optimize ATP loading to nZVI, we prepared materials at different mass ratios of nZVI to ATP (1 : 0.5, 1 : 1, 1 : 3, and 1 : 5) and obtained NO_3-N removal rates of 70.57%, 78.61%, 71.74%, and 61.49%, respectively (Figure 5). The highest ratios of

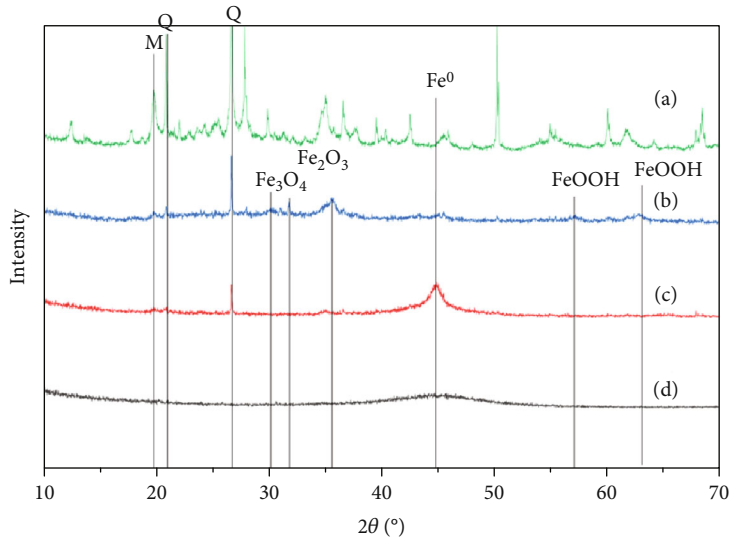

Figure 2: XRD images of (a) ATP, (b) nitrate-laden ATP-nZVI, (c) ATP-nZVI, and (d) nZVI. ATP: attapulgite; ATP-nZVI: nano-zero-valent iron-coated attapulgite; nZVI: nano-zero-valent iron.

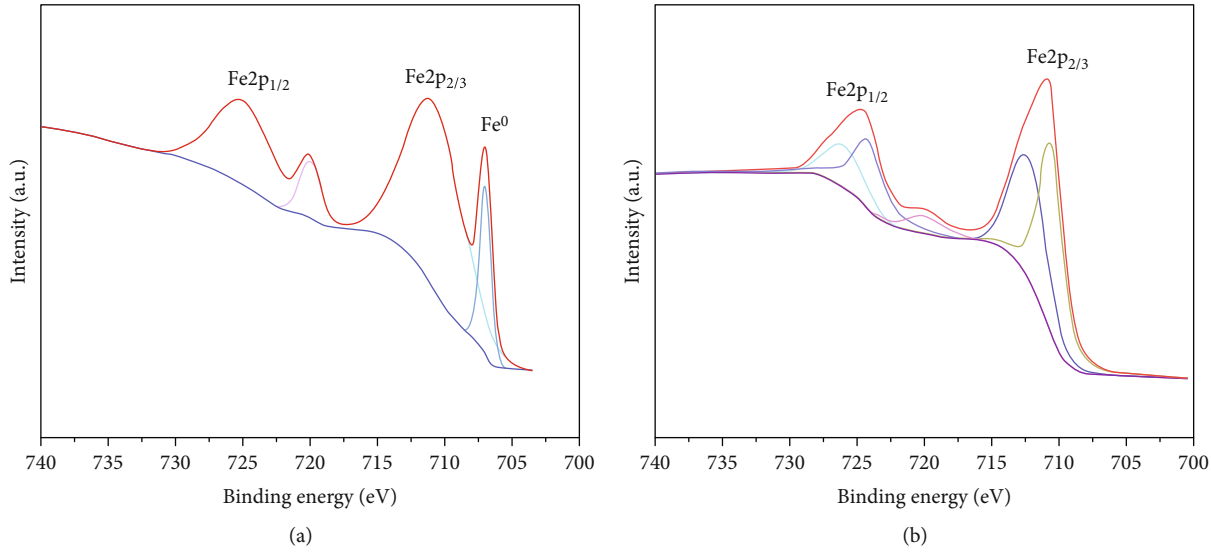

Figure 3: X-ray photoelectron spectroscopy spectra (a) before and (b) after NO_3-N removal by ATP-nZVI. ATP-nZVI: nano-zero-valent iron-coated attapulgite.

nZVI (nZVI to ATP mass ratio = 1 : 0.5) and ATP (nZVI to ATP mass ratio = 1 : 5) did not achieve the maximum NO_3-N removal rate. Instead, the NO_3-N removal rate peaked when the nZVI to ATP mass ratio was 1 : 1. Notably, when nZVI dosage in the composite was not significantly different from that of ATP, the NO_3-N removal efficiency was relatively high, indicating that nZVI plays an important role in the NO_3-N removal. However, when the ATP dosage was further increased and the mass ratio of nZVI to ATP was increased from 1 : 3 to 1 : 5, the active nZVI sites were encapsulated, reducing the loading effect of ATP on nZVI, thereby reducing the ATP, number of surface functional groups, and reactive sites on the nZVI composites, which reduced their ability to remove NO_3-N.

Additionally, comparing the effects of nZVI and ATP-nZVI revealed that ATP loading effectively inhibited the production of ammonia nitrogen. Studies have reported that most products of NO_3-N reduction via zero-valent iron include ammonia nitrogen [14], which is consistent with our findings. With an increase in the ATP loading ratio, the ammonia nitrogen production decreased slightly from 57.45% at 1 : 0.5 to 51.04% at 1 : 5. Following nitrate nitrogen generation, the production rate accounted for a small proportion of the total nitrogen. Therefore, the optimal mass ratio of nZVI to ATP was determined to be 1 : 1.

3.4. Effect of Initial pH. To explore the effect of the initial pH on NO_3-N removal from groundwater by ATP-nZVI, the

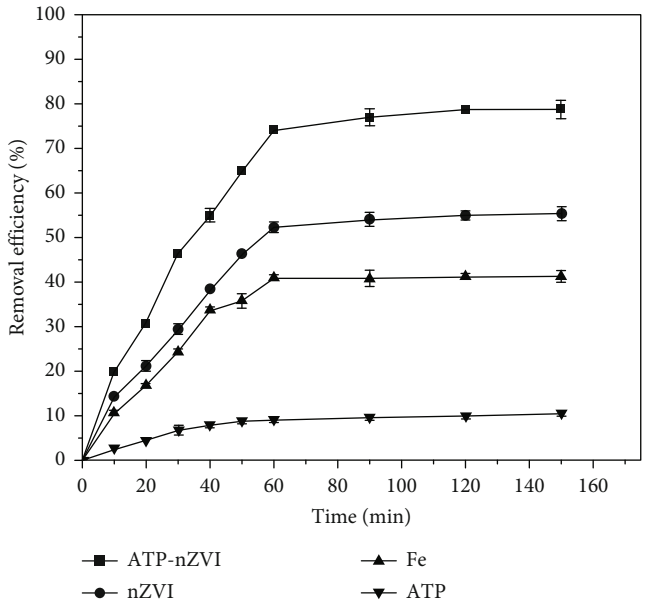

Figure 4: NO_3-N removal rates for different materials (ATP, Fe, nZVI, and ATP-nZVI). ATP: attapulgite; ATP-nZVI: nano-zero-valent iron-coated attapulgite; nZVI: nano-zero-valent iron (initial NO_3-N concentration = 30 mg/L, adsorbent = 1.5 g/L, pH = 7, reaction temperature = 25°C, and contact time = 150 min).

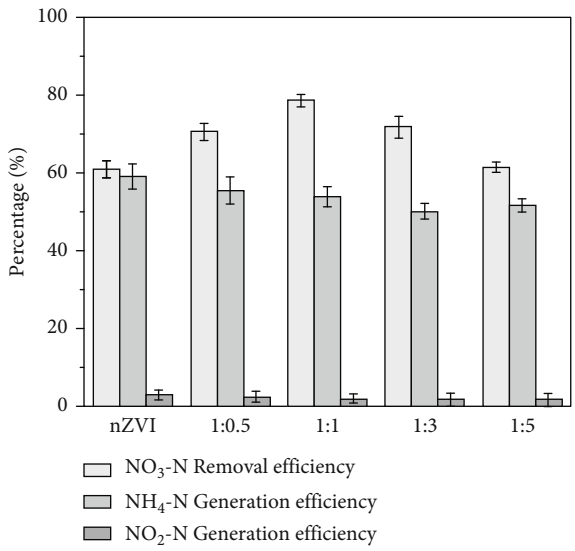

Figure 5: Effect of nZVI and ATP mass ration on NO_3-N removal rate. ATP: attapulgite; nZVI: nano-zero-valent iron (initial NO_3-N concentration = 30 mg/L, adsorbent = 1.5 g/L, pH = 7, reaction temperature = 25°C, and contact time = 150 min).

initial pH was set at 3, 5, 7, and 9 using NaOH and HCl, as required. We achieved NO_3-N removal rates of 79.77%, 79.58%, 78.61%, and 74.27%, respectively. The removal rate did not change significantly when the reaction reached equilibrium under different pH conditions (Figure 6). When the pH values were 3 and 5, equilibrium was reached within 50 min and the removal rates were 79.77% and 79.58%, respectively. When the pH value was 7, the removal rate

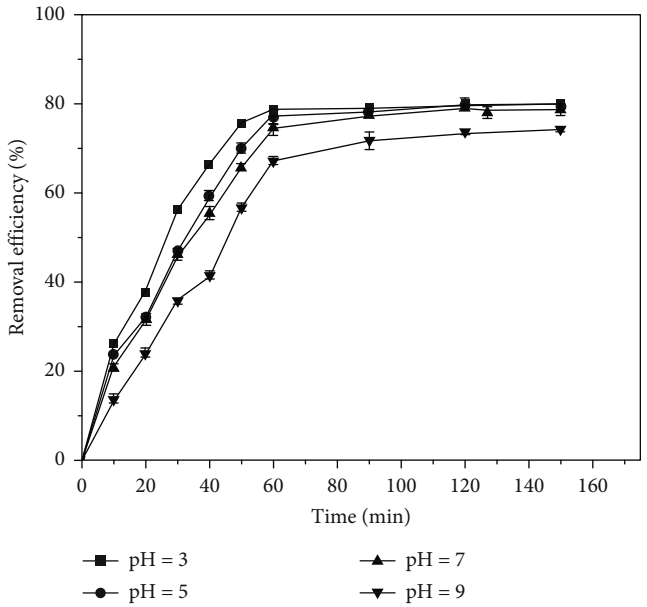

Figure 6: Effect of changes in initial pH on NO_3-N removal rate (initial NO_3-N concentration = 30 mg/L, adsorbent = 1.5 g/L, reaction temperature = 25°C, and contact time = 150 min).

was 78.61% at 90 min. At a pH 9, equilibrium was reached at 120 min, with a removal rate of 74.27%; however, the increase in pH negatively correlated with the reaction rate. This is because the stronger the acidity, the higher the reduction rate due to the acceleration of H^+ ions [37]. Therefore, under this condition, it is easier for nZVI to lose electrons and be oxidized, whereas it is easier for NO_3-N to gain electrons and be reduced [20, 22, 38]. In contrast, alkaline conditions increase the oxides on the nZVI surface, hindering the reducing agents and target contaminants. As the reaction progressed, corrosive products, such as hydroxides, generated in the solution gradually precipitated on the particle surface, thus limiting the nitrate diffusion from nZVI particle surface to the inner layer [39]. These results showed NO_3-N reduction by nZVI is an acid-driven reaction.

3.5. Effect of Initial Temperature. Water temperature is an important factor affecting chemical reactions; therefore, investigating the effect of temperature changes on NO_3-N removal is necessary. The increase in the temperature positively correlated with NO_3-N removal efficiency, although the removal efficiency did not change significantly (Figure 7). At reaction equilibrium, the removal rates at 15, 25, and 35°C were 75.81%, 78.61%, and 80.32%, respectively. At 35°C, the reaction reached equilibrium at 60 min, whereas at the other temperatures, it reached equilibrium at 100 min. The results showed that NO_3-N removal rates increased slightly with increasing water temperature. This was attributed to the fact that increase in the temperature accelerated the rate of intermolecular movement, thereby increasing the probability of nitrate contacting nZVI and being removed faster. Additionally, an increase in the reaction temperature increased the activation energy of the chemical reaction, which aided in overcoming the reaction energy

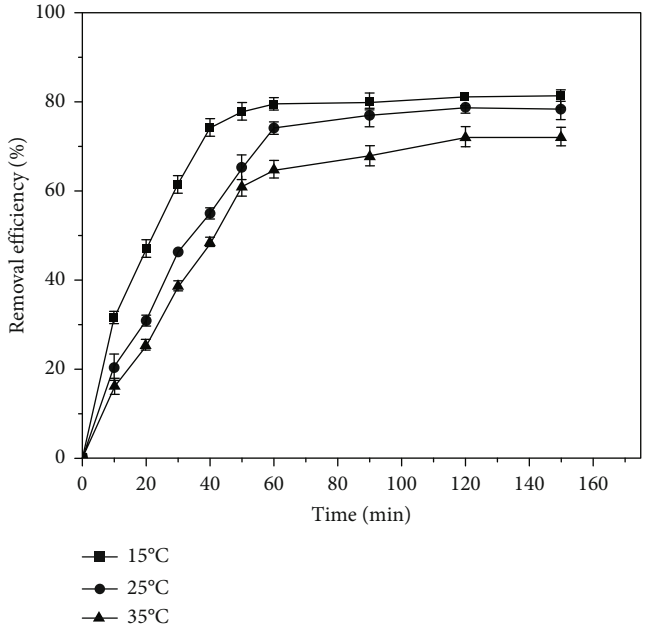

Figure 7: Effect of initial temperature on NO_3-N removal rate (initial NO_3-N concentration = 30 mg/L, adsorbent = 1.5 g/L, pH = 7, and contact time = 150 min).

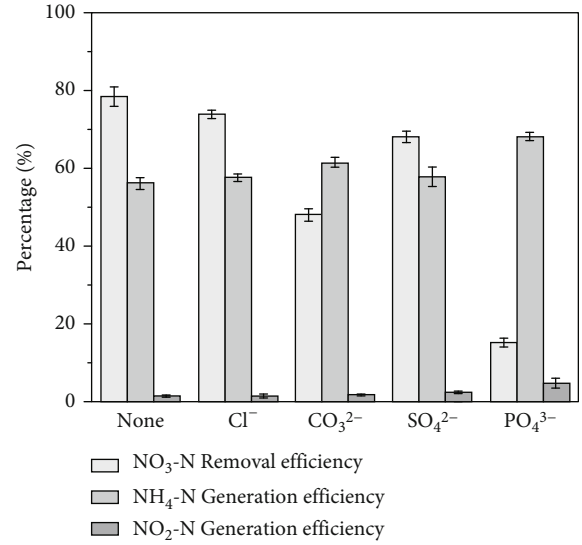

Figure 8: Rates of NO_3-N removal and ammonia nitrogen and nitrite generation in presence of coexisting ions (anion concentration to nitrate nitrogen ion ratio = 4 : 1, mass ratio of ATP-nZVI material = 1 : 1, initial NO_3-N concentration = 30 mg/L, adsorbent = 1.5 g/L, pH = 7, reaction temperature = 25°C, and contact time = 150 min).

barrier [40], thus promoting the reaction process. This result is consistent with those of studies that utilized zero-valent iron to degrade pollutants [41, 42]. Our results confirmed that the increase in the temperature aided NO_3-N removal [43].

3.6. Role of Coexisting Anions. Different anions coexist in groundwater, which may interfere with NO_3-N removal by ATP-nZVI. To assess the influence of coexisting anions in an actual water body on the reaction system, samples containing PO_4^{3-}, SO_4^{2-}, Cl^-, CO_3^{2-}, and a blank control were used, where the ratio of the anion concentration to the nitrate nitrogen ion was 4 : 1. The order of NO_3-N removal inhibition by ATP-nZVI due to various coexisting anions was $PO_4^{3-}>CO_3^{2-}>SO_4^{2-}>Cl^-$ (Figure 8). Here, PO_4^{3-} had the greatest effect on NO_3-N removal as its presence decreased NO_3-N removal efficiency sharply from 78.64% to 15.2%. Owing to the strong binding ability of CO_2^{3-} to the ATP surface, iron, as a reducing agent, reacted with PO_4^{3-}, thus reducing the probability of NO_3^- being adsorbed on the iron surface. NO_3^- removal rate decreased when these anions coexist in large amounts. The presence of CO_2^{3-} also partially inhibited the reaction, and the removal rate decreased to 48.32%. The presence of Cl^- and SO_4^{2-} had a negligible effect on NO_3-N removal, with removal rates being 74.23% and 68.44%, respectively. Additionally, NO_3^- formed precipitates with the corrosion products, i.e., Fe(II)/Fe(III), adsorbed on the iron surface.

The presence of coexisting anions (NO_3-N, PO_4^{3-}, SO_4^{2-}, Cl^-, and CO_3^{2-}) in water body slightly increased the conversion of ammonia nitrogen compared with the control, with conversion rates of 68.25%, 58.12%, 57.65%, 61.74%, and 56.32%, respectively. These results suggest that coexisting surface ions promote the formation of ammonia nitrogen.

3.7. Adsorption Kinetic Model. The kinetics of ATP-nZVI were fitted using pseudosecond-order models at different initial pH values, temperatures, and coexisting anions. The fitting parameters are provided in the Supporting Information (Tables S1, S2, and S3). The results showed that ATP-nZVI kinetics can optimally fit a pseudosecond-order model.

In the pseudosecond-order model fitting at different initial pH values, the larger pseudosecond-order kinetic reaction constant and faster the reaction rate were obtained at lower pH; the optimal pH was 3 with the fitting result of R^2 = 0.996 (Figure S1). The fitting of the pseudosecond-order model at different initial temperatures showed that greater pseudosecond-order kinetic reaction constant and faster reaction rates were obtained at higher temperatures (Figure S2). The higher temperature is beneficial for the accelerated molecular movement. The pseudosecond-order model fitting in the presence of coexisting anions (Figure S3) exhibited a faster reaction rate than that under other anions in the presence of Cl^-, whereas the presence of PO_4^{3-} led to a rapid decrease in the reaction rate.

3.8. NO_3-N Removal Mechanism. Based on the characterization and batch experiments, Figure 9 summarizes the reaction mechanism of nZVI-mediated NO_3-N removal on the surface of the ATP-nZVI composite, where nZVI was oxidized to Fe(II) and Fe(III) by electrostatic attraction and chemisorption of NO_3-N on the surface, followed by its further reduction. The chemical adsorption of electrons exchanged between NO_3-N and ATP-nZVI is the main rate-limiting step in the nitrogen-nitrate removal reaction process [44]. This result further demonstrated that the physical diffusion and electron exchange between the adsorbent and adsorbate contributes to the reaction during NO_3-N removal by ATP-nZVI. The reactions are shown in Equations (4)–(7).

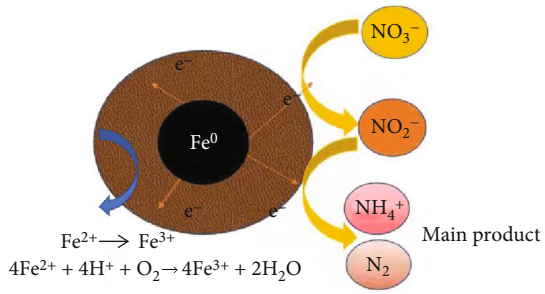

Figure 9: NO_3-N removal mechanism of nZVI. ATP: attapulgite; nZVI: nano-zero-valent iron.

Altered NO_3-N removal by ATP-nZVI in an aqueous solution was due to the incomplete removal of air; as a result, ATP-nZVI reacted with dissolved oxygen to produce Fe(II) (see Equation (3)). The change in the pH value, which increased rapidly (Figure 10), was due to the production of a large amount of hydroxide during the reaction [45]. The pH of the solution finally remained between 9.0 and 9.5; the alkaline condition was conducive to the precipitation of ferrous iron and reduced secondary pollution caused by the dissolution of soluble iron [20, 22, 38], consistent with the results of previous studies.

Figure 11 shows the variation in the nitrogen species concentration with time under the experimental conditions. Nitrite was detected only in the early stage, peaking at 40 min, and then decreased slightly. As reaction progressed, ammonia nitrogen increased to 12.71 mg/L, whereas the total nitrogen decreased to 17.64 mg/L, indicating that ammonia nitrogen and nitrogen were the main products of the reduction process. The nitrite was only the intermediate product of the NO_3-N reduction reaction and was subsequently converted to ammonia nitrogen and nitrogen [10, 46]. The reaction equations are as follows:

$$Fe^0 + O_2 + H_2O \longrightarrow 2Fe^{2+} + 4OH^-, \quad (3)$$

$$Fe^0 + NO_3^- + 2H^+ \longrightarrow Fe^{2+} + H_2O + NO_2^-, \quad (4)$$

$$3Fe^0 + NO_2^- + 8H^+ \longrightarrow 3Fe^{2+} + 2H_2O + NH_4^+, \quad (5)$$

$$3Fe^0 + 2NO_2^- + 8H^+ \longrightarrow 3Fe^{2+} + 4H_2O + N_2\uparrow, \quad (6)$$

$$5Fe^0 + 2NO_3^- + 6H_2O \longrightarrow 5Fe^{2+} + 12OH^- + N_2\uparrow. \quad (7)$$

Iron is oxidized mainly on particle surfaces and generates iron oxides and hydroxides. The main accompanying reactions were as follows:

$$Fe^{2+} + 2OH^- \longrightarrow Fe(OH)_2, \quad (8)$$

$$4Fe^{2+} + O_2 + 4H_2O \longrightarrow 2Fe_2O_3 + 8H^+, \quad (9)$$

$$4Fe^{2+} + O_2 + 4H^+ \longrightarrow 4Fe^{3+} + 2H_2O, \quad (10)$$

$$Fe^{3+} + 3OH^- \longrightarrow Fe(OH)_3, \quad (11)$$

$$Fe(OH)_3 + 3H^+ \longrightarrow FeOOH + H_2O. \quad (12)$$

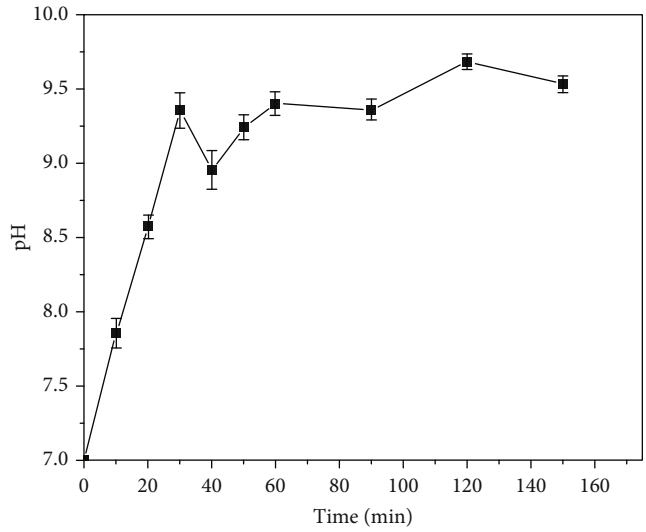

Figure 10: Change in pH during NO_3-N removal by ATP-nZVI. nZVI: nano-zero-valent iron.

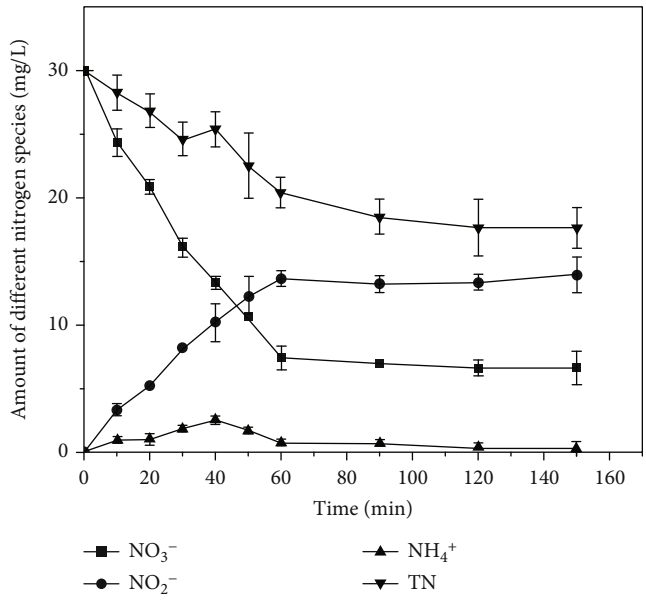

Figure 11: Change in nitrogen species over time.

During the reduction of nitrate solution using ATP-nZVI, the total number of nitrogen species decreased compared with the initial number, indicating that part of the nitrogen from the aqueous phase was converted to the gas phase while part of the nitrogen in the solution was converted to gaseous nitrogen, which escaped [47]. According to the principle of mass balance, including that for water and gas species, a small decrease in the total nitrogen volume led to the escape of gases. Alternatively, a small amount of solid residue adsorption was observed. This also indicated that during nitric acid treatment by ATP-nZVI, a large amount of NO_3-N was converted to other nitrogen species. Therefore, the main reason for NO_3-N removal by ATP-

nZVI was the reduction of nZVI, where ATP loading improved the reduction efficiency. Compared with similar studies (Table 1), ATP-nZVI showed a good NO_3-N removal rate at low cost.

4. Conclusions

In this study, an ATP-nZVI composite was successfully prepared and used for the efficient removal of NO_3-N from groundwater. The stability of ATP-nZVI and its NO_3-N removal performance were evaluated. The changes in the surface, composition, and properties of the material before and after the reaction of ATP-nZVI with nitrate were investigated. A variety of materials (iron powder, ATP, nZVI, and ATP-nZVI) were compared to verify the advantages of ATP-nZVI for NO_3-N removal. Additionally, the effects of nZVI on the ATP mass ratio, initial pH value, water temperature, and coexisting anions on the removal of NO_3-N from groundwater via ATP-nZVI were investigated.

Based on the characterization results, we inferred that the aluminum silicate particles in the ATP structure are effective carriers of nZVI, which promote the crystallization of the reaction product and reduce self-consumption caused by the oxidation and aggregation of nZVI. Compared with nZVI, ATP-nZVI is more stable in aqueous solutions and less prone to oxidation and aggregation. The removal order of NO_3-N with respect to the different preparation materials was ATP-nZVI>nZVI>iron powder>ATP. During the removal of NO_3-N by ATP-nZVI, most of the NO_3-N was converted into NH_4-N, N_2 was generated, and the pH increased. In terms of the mass ratio of nZVI to ATP, the loading mass ratio between nZVI and ATP was optimized; the removal efficiency of NO_3-N was highest when the ratio of nZVI to ATP was 1 : 1. The initial pH had a rate limiting effect on NO_3-N removal; therefore, the equilibration was reached faster when the solution was acidic than when it was alkaline. However, the NO_3-N removal rate could be promoted by increasing the reaction temperature. The order of the inhibitory effect of the coexisting anions on NO_3-N removal was PO_3^{4-}>CO_3^{2-}>SO_2^{4-}>Cl^-. The ATP-nZVI synthesis process used in this study is simple, environmentally friendly, and cost-effective and can efficiently treat NO_3-N-contaminated water and wastewater. Thus, it is a promising material to treat contaminated groundwater. In the future, more research studies should be conducted on ATP-nZVI composites because the actual NO_3-N removal efficiency in groundwater may be affected by other factors not evaluated in this study, such as microorganisms and water velocity; such studies will be useful to completely understand the corresponding underlying mechanisms and processes.

Data Availability

The data used to support the findings of this study are included within the article and supplementary information files.

Conflicts of Interest

The authors declare that they have no conflicts of interest.

Acknowledgments

This work was supported by the Natural Science Foundation of Chongqing, China (cstc2021jcyj-bshX0231, cstc2020jcyj-msxmX0763, and cstc2021jcyj-msxmX0328).

Supplementary Materials

Table S1 lists the kinetic fitting parameters of nitrate removal by ATP-nZVI at different initial pH values. Table S2 lists the kinetic fitting parameters of nitrate removal by ATP-nZVI at different initial temperatures. Table S3 lists the kinetic fitting parameters of nitrate removal in the presence of coexisting anions using ATP-nZVI. Figures S1, S2, and S3 show the kinetics of ATP-NZVI at different initial pH values, initial temperatures, and coexisting anions, respectively. *(Supplementary Materials)*

References

[1] E. Elisante and A. N. N. Muzuka, "Occurrence of nitrate in Tanzanian groundwater aquifers: a review," *Applied Water Science*, vol. 7, no. 1, pp. 71–87, 2017.

[2] J. Xin, Y. Wang, Z. L. Shen, Y. Liu, H. T. Wang, and X. Zheng, "Critical review of measures and decision support tools for groundwater nitrate management: a surface-to-groundwater profile perspective," *Journal of Hydrology*, vol. 598, article 126386, 2021.

[3] M. M. Azadegan, M. R. A. Moghaddam, and R. Maknoon, "Public awareness and performance regarding nitrate pollution in nitrate-polluted area of Tehran, Iran," *Environmental Engineering and Management Journal*, vol. 13, no. 3, pp. 611–617, 2014.

[4] A. D. van den Brand, M. Beukers, M. Niekerk et al., "Assessment of the combined nitrate and nitrite exposure from food and drinking water: application of uncertainty around the nitrate to nitrite conversion factor," *Food Additives & Contaminants: Part A*, vol. 37, no. 4, pp. 568–582, 2020.

[5] J. Chen, Q. Huang, Y. Lin et al., "Hydrogeochemical characteristics and quality assessment of groundwater in an irrigated region Northwest China," *Water*, vol. 11, no. 1, p. 96, 2019.

[6] A. M. E. Khalil, O. Eljamal, T. W. M. Amen, Y. Sugihara, and N. Matsunaga, "Optimized nano-scale zero-valent iron supported on treated activated carbon for enhanced nitrate and phosphate removal from water," *Chemical Engineering Journal*, vol. 309, pp. 349–365, 2017.

[7] C. A. Schmidt and M. W. Clark, "Efficacy of a denitrification wall to treat continuously high nitrate loads," *Ecological Engineering*, vol. 42, pp. 203–211, 2012.

[8] Z. Yang, C. Shan, Y. C. Mei, Z. Jiang, X. H. Guan, and B. C. Pan, "Improving reductive performance of zero valent iron by H_2O_2/HCl pretreatment: a case study on nitrate reduction," *Chemical Engineering Journal*, vol. 334, pp. 2255–2263, 2018.

[9] L. Di Palma, N. Verdone, and G. Vilardi, "Kinetic modeling of Cr(VI) reduction by nZVI in soil: the influence of organic matter and manganese oxide," *Bulletin of Environmental Contamination and Toxicology*, vol. 101, no. 6, pp. 692–697, 2018.

[10] J. H. Zhang, Z. W. Hao, Z. Zhang, Y. P. Yang, and X. H. Xu, "Kinetics of nitrate reductive denitrification by nanoscale zero-valent iron," *Process Safety and Environmental Protection*, vol. 88, no. 6, pp. 439–445, 2010.

[11] X. Zhao, W. Liu, Z. Cai, B. Han, T. Qian, and D. Zhao, "An overview of preparation and applications of stabilized zero-valent iron nanoparticles for soil and groundwater remediation," *Water Research*, vol. 100, pp. 245–266, 2016.

[12] L. Zhong, Y. X. Feng, G. Y. Wang et al., "Production and use of immobilized lipases in/on nanomaterials: a review from the waste to biodiesel production," *International Journal of Biological Macromolecules*, vol. 152, pp. 207–222, 2020.

[13] Y. Vicente-Martinez, M. Caravaca, A. Soto-Meca, M. A. Martin-Pereira, and M. D. Garcia-Onsurbe, "Adsorption studies on magnetic nanoparticles functionalized with silver to remove nitrates from waters," *Water*, vol. 13, no. 13, p. 1757, 2021.

[14] H. Y. Liu, M. Guo, and Y. Zhang, "Nitrate removal by Fe-0/Pd/Cu nano-composite in groundwater," *Environmental Technology*, vol. 35, no. 7, pp. 917–924, 2014.

[15] A. Ghosh, N. K. Meshram, and R. Saha, "Glycerol-mediated synthesis of nanoscale zerovalent iron and its application for the simultaneous reduction of nitrate and alachlor," *Environmental Science and Pollution Research*, vol. 26, no. 12, pp. 11951–11961, 2019.

[16] W. D. Liang, R. Wang, C. J. Wang et al., "Facile preparation of attapulgite-based aerogels with excellent flame retardancy and better thermal insulation properties," *Journal of Applied Polymer Science*, vol. 136, no. 32, p. 47849, 2019.

[17] J. H. Wang and D. J. Chen, "Mechanical properties of natural rubber nanocomposites filled with thermally treated attapulgite," *Journal of Nanomaterials*, vol. 2013, Article ID 496584, p. 11, 2013.

[18] N. Guo, J. S. Wang, J. Li, Y. G. Teng, and Y. Z. Zhai, "Dynamic adsorption of Cd2+ onto acid-modified attapulgite from aqueous solution," *Clays and Clay Minerals*, vol. 62, no. 5, pp. 415–424, 2014.

[19] J. H. Huang, Y. F. Liu, Q. Z. Jin, X. G. Wang, and J. Yang, "Adsorption studies of a water soluble dye, Reactive red MF-3B, using sonication-surfactant-modified attapulgite clay," *Journal of Hazardous Materials*, vol. 143, no. 1-2, pp. 541–548, 2007.

[20] N. Q. Zhang, J. Y. Chen, Z. Q. Fang, and E. P. Tsang, "Ceria accelerated nanoscale zerovalent iron assisted heterogenous Fenton oxidation of tetracycline," *Chemical Engineering Journal*, vol. 369, pp. 588–599, 2019.

[21] W. Y. Zhang, L. B. Qian, Y. Chen et al., "Nanoscale zero-valent iron supported by attapulgite produced at different acid modification: synthesis mechanism and the role of silicon on Cr(VI) removal," *Chemosphere*, vol. 267, 2020.

[22] W. Y. Zhang, L. B. Qian, D. Ouyang, Y. Chen, L. Han, and M. F. Chen, "Effective removal of Cr(VI) by attapulgite-supported nanoscale zero-valent iron from aqueous solution: enhanced adsorption and crystallization," *Chemosphere*, vol. 221, pp. 683–692, 2019.

[23] L. Dong, L. Lin, Q. Y. Li et al., "Enhanced nitrate-nitrogen removal by modified attapulgite-supported nanoscale zero-valent iron treating simulated groundwater," *Journal of Environmental Management*, vol. 213, pp. 151–158, 2018.

[24] Z. J. Wang, Z. Wang, K. Xu, L. Chen, Z. Z. Liu, and Y. L. Liu, "Denitrification performance and kinetics of an attapulgite lightweight ceramsite biofilter," *Desalination and Water Treatment*, vol. 178, pp. 110–122, 2020.

[25] H. D. Wu, J. W. Wang, H. Liu, and X. Y. Fan, "Performance, reaction pathway and kinetics of the enhanced dechlorination degradation of 2,4-dichlorophenol by Fe/Ni nanoparticles supported on attapulgite disaggregated by a ball milling–freezing process," *Materials*, vol. 15, no. 11, p. 3957, 2022.

[26] Y. Zhang, J. Shen, Q. Li et al., "Development and characterization of co-polyimide/attapulgite nanocomposites with highly enhanced thermal and mechanical properties," *Polymer Composites*, vol. 35, no. 1, pp. 86–96, 2014.

[27] J. Jiang, W. Liu, J. T. Chen, and Y. L. Hou, "LiFePO4 nanocrystals: liquid-phase reduction synthesis and their electrochemical performance," *ACS Applied Materials & Interfaces*, vol. 4, no. 6, pp. 3062–3068, 2012.

[28] C. Q. Li, S. S. Yang, R. Z. Bian et al., "Efficient catalytic degradation of bisphenol A coordinated with peroxymonosulfate via anchoring monodispersed zero-valent iron on natural kaolinite," *Chemical Engineering Journal*, vol. 448, article 137746, 2022.

[29] C. Tissen, S. A. Benz, K. Menberg, P. Bayer, and P. Blum, "Groundwater temperature anomalies in Central Europe," *Environmental Research Letters*, vol. 14, no. 10, article 104012, 2019.

[30] M. C. Ciardelli, H. F. Xu, and N. Sahai, "Role of Fe(II), phosphate, silicate, sulfate, and carbonate in arsenic uptake by coprecipitation in synthetic and natural groundwater," *Water Research*, vol. 42, no. 3, pp. 615–624, 2008.

[31] MEP (Ministry of Environmental Protection P R China), *Water Quality-Determination of Nitrate-Nitrogen-Ultraviolet Spectrophotometry (HJ/T346-2007)*, MEP, Beijing, 2007.

[32] R. Fu, Y. Yang, Z. Xu, X. Zhang, X. Guo, and D. Bi, "The removal of chromium (VI) and lead (II) from groundwater using sepiolite- supported nanoscale zero-valent iron (S-NZVI)," *Chemosphere*, vol. 138, pp. 726–734, 2015.

[33] L. N. Shi, X. Zhang, and Z. L. Chen, "Removal of chromium (VI) from wastewater using bentonite-supported nanoscale zero-valent iron," *Water Research*, vol. 45, no. 2, pp. 886–892, 2011.

[34] L. Qian, W. Zhang, J. Yan et al., "Nanoscale zero-valent iron supported by biochars produced at different temperatures: synthesis mechanism and effect on Cr(VI) removal," *Environmental Pollution*, vol. 223, pp. 153–160, 2017.

[35] Y. M. Su, A. S. Adeleye, Y. X. Huang, X. F. Zhou, A. A. Keller, and Y. L. Zhang, "Direct synthesis of novel and reactive sulfide-modified nano iron through nanoparticle seeding for improved cadmium-contaminated water treatment," *Scientific Reports*, vol. 6, 2016.

[36] S. Bakshi, C. Banik, S. J. Rathke, and D. A. Laird, "Arsenic sorption on zero-valent iron-biochar complexes," *Water Research*, vol. 137, no. 15, pp. 153–163, 2018.

[37] X. H. Guan, Y. K. Sun, H. J. Qin et al., "The limitations of applying zero-valent iron technology in contaminants sequestration and the corresponding countermeasures: the development in zero- valent iron technology in the last two decades (1994-2014)," *Water Research*, vol. 75, pp. 224–248, 2015.

[38] Y. Zhou and X. F. Li, "Green synthesis of modified polyethylene packing supported tea polyphenols- NZVI for nitrate removal from wastewater: characterization and mechanisms," *Science of the Total Environment*, vol. 806, Part 2, article 150596, 2022.

[39] L. Yong and W. Jianlong, "Reduction of nitrate by zero valent iron (ZVI)-based materials: a review," *Science of the Total Environment*, vol. 671, pp. 388–403, 2019.

[40] S. Ghosh, S. Hariharan, and A. K. Tiwari, "Water adsorption and dissociation on copper/nickel bimetallic surface alloys: effect of surface temperature on reactivity," *The Journal of Physical Chemistry C*, vol. 121, no. 30, pp. 16351–16365, 2017.

[41] M. Arshadi, M. Soleymanzadeh, J. W. L. Salvacion, and F. SalimiVahid, "Nanoscale zero-valent iron (NZVI) supported on *sineguelas* waste for Pb(II) removal from aqueous solution: kinetics, thermodynamic and mechanism," *Journal of Colloid and Interface Science*, vol. 426, pp. 241–251, 2014.

[42] F. Zhu, S. Y. He, and T. Liu, "Effect of pH, temperature and co-existing anions on the removal of Cr(VI) in groundwater by green synthesized nZVI/Ni," *Ecotoxicology and Environmental Safety*, vol. 163, pp. 544–550, 2018.

[43] N. L. Hoover, A. Bhandari, M. L. Soupir, and T. B. Moorman, "Woodchip denitrification bioreactors: impact of temperature and hydraulic retention time on nitrate removal," *Journal of Environmental Quality*, vol. 45, no. 3, pp. 803–812, 2016.

[44] X. Tan, Y. Liu, G. Zeng et al., "Application of biochar for the removal of pollutants from aqueous solutions," *Chemosphere*, vol. 125, pp. 70–85, 2015.

[45] H. L. Lu, H. Xu, Y. Chen, J. L. Zhang, and J. X. Zhuang, "ZVI/PANI/ATP composite by static polymerization as adsorbent for removal of Cr(VI)," *Rsc Advances*, vol. 4, no. 12, pp. 5873–5879, 2014.

[46] W. Wei, J. Zhao-hui, L. Tie-long, Z. Huan, and G. Si, "Preparation of spherical iron nanoclusters in ethanol-water solution for nitrate removal," *Chemosphere*, vol. 65, pp. 1396–1404, 2006.

[47] Z. Yun, L. Yimin, L. Jianfa, H. Liujiang, and Z. Xuming, "Enhanced removal of nitrate by a novel composite: nanoscale zero valent iron supported on pillared clay," *Chemical Engineering Journal*, vol. 171, no. 2, pp. 526–531, 2011.

[48] C. C. Y. Gordon and L. Hsaio-Lan, "Chemical reduction of nitrate by nanosized iron: kinetics and pathways," *Water Research*, vol. 39, pp. 884–894, 2005.

[49] N. Song, Z. Chen, J. Shi, D. Shi, and L. Gu, "Performance and mechanism of chelating resin (TP-207) supported Pd/Cu bimetallic nanoparticles in selective reduction of nitrate by using ZVI (zero valent iron) as reductant," *Separation and Purification Technology*, vol. 272, 2021.

[50] F. Fatemeh Sadat and F. Cavus, "Zero valent nano-sized iron/clinoptilolite modified with zero valent copper for reductive nitrate removal," *Process Safety and Environmental Protection*, vol. 91, pp. 304–310, 2013.

[51] L. Guo, Z. Yaqi, L. Zhaoyang et al., "Efficient nitrate removal using micro-electrolysis with zero valent iron/activated carbon nanocomposite," *Journal of Chemical Technology and Biotechnology*, vol. 91, no. 12, pp. 2942–2949, 2016.

[52] S. Sepehri, M. Heidarpour, and J. Abedi-Koupai, "Nitrate removal from aqueous solution using natural zeolite-supported zero-valent iron nanoparticles," *Soil and Water Research*, vol. 9, no. 4, pp. 224–232, 2014.